Scanning-tunneling-microscope investigation of a 215-MeV Ne-irradiated graphite surface

L. P. Biró and J. Gyulai
KFKI–Research Institute for Materials Science, H-1525 Budapest, P.O. Box 49, Hungary

K. Havancsák
Institute for Solid State Physics of Eötvös University, H-1088 Budapest, Múzeum krt. 6-8, Hungary
(Received 13 February 1995)

Surface structure on highly oriented pyrolithic graphite irradiated by low-dose 215-MeV Ne ions was investigated by scanning tunneling microscopy. Three types of surface features were found: ones produced by low-energy knocked-on C atoms (type I, ones produced by high-energy knocked-on C atoms emerging from the irradiated surface of the target (type II), and a defect attributed to knocked-on C atom with energy around the maximum of electronic stopping moving in a direction approximatively parallel to the irradiated surface (type III). In some instances, atomic resolution was achieved on the observed surface features. Structures, which can be ascribed to entering of the Ne ions themselves, were not found.

INTRODUCTION

The effects of irradiation on graphite were extensively investigated some 30 years ago.[1] The strong interest in radiation damage in graphite was motivated by its usage in nuclear reactors. A renewal of interest in the study of irradiated graphite is due to the possibility offered by scanning probe methods to investigate on an atomic scale the individual features produced by impact on energetic particles. Several authors investigated the surface structures produced by low-, medium-, and high-energy projectiles on graphite.[2–7] There is general agreement that irradiation with energetic particles produces small protrusions, called hillocks, with a diameter of a few nm and with a height in the Å range. The exact origin of these features has not been satisfactorily explained. One of the most frequently used explanations is based on the intercalation of interstitials between two adjacent graphite layers. An alternative explanation proposed[7] is that, in the case of 530-keV and 4.5-MeV Au-bombarded HOPG (highly oriented pyrolithic graphic), the hillocks are due to a Coulomb explosion, and that smaller features, called bumps are generated by knocked-on C atoms which have a trajectory intersecting the irradiated surface. The Coulomb explosion is a damage-producing mechanism based on the repulsive forces between the nuclei that have lost of their electrons due to interaction with the penetrating ion.[8] This mechanism is recognized for damage produced in insulators by swift particles[9] and in the last few years experimental evidence has also been reported for some metals.[10–12] Most investigators agree that the spatial region modified directly by energy released by the penetrating ion due to electronic stopping is of cylindrical shape with a dense core of defects approximatively 10 nm in diameter, and an influenced region with diameter in the range of 100 nm.[9,12] In this case, one would expect some regularity in the shape of features produced by electronic stopping effects, and a better dimensional correlation between the diameter of the hillocks and the electronic cascade. On the other hand, the bumps, which are attributed to knocked-on C atoms with energies in the nuclear stopping range,[7] are just slightly different compared to the hillocks attributed to electronic effects. This would mean that the two different damage-producing mechanisms yield very similar damage structures.

In an attempt to try to elucidate the nature of surface features found on ion-irradiated graphite, HOPG irradiated with 215-MeV Ne was investigated by scanning tunneling microscopy (STM). Three different kinds of surface structures were found: irregularly shaped hillocks with irregular height distribution, regularly shaped elliptical features with constant height and well-developed craters, and a regular superstructure over several hundreds of nm.

EXPERIMENT

Bulk HOPG was irradiated in a direction normal to the *c plane* of graphite with 215-MeV Ne ions from the U-400 cyclotron in Dubna. A low dose of 10^{12} Ne/cm^2 was used, so that cascade overlapping in the surface region may be ruled out. This means that all the observed structures originate from individual ion impacts. Irradiation was carried out in air, and the increase of sample temperature during irradiation was less than 15 °C.

Samples were imaged by STM in a constant current mode, in air, using 1-nA and 100-mV tunneling conditions with scanning speeds usually in the range of 100–3000 nm/s. Mechanically prepared Pt-Rh tips were used, and the tip quality was periodically checked over undamaged regions of the same sample.

The density of surface features that could be unambiguously attributed to ionic impacts was approximately 5×10^{-7} nm^{-2}, i.e., 5×10^{-5} features/ion. In some cases closely grouped hillocks were found over regions of 300×300 nm^2; these were considered as one single event, as they very likely originated from a single knocked-on C atom. The simulation using the TRIM code,[13] with a dis-

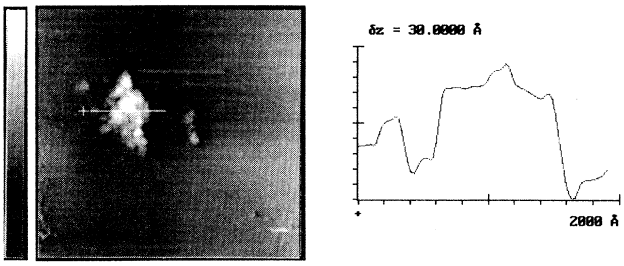

a) b)

FIG. 1. Gray scale STM image; window of 6100×6100 Å^2; z range: 35 Å. The gray scale on the left side corresponds to the whole z range. (a) Plan view of a type-I structure. (b) Line cut along the white line in (a); the cross indicates the starting point.

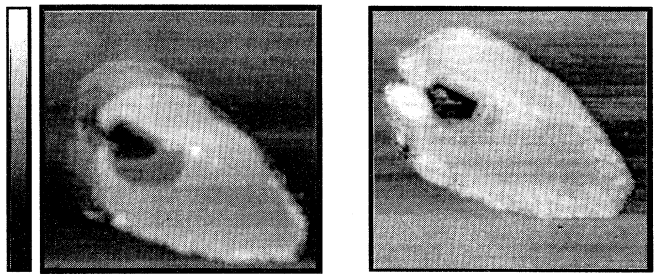

a) b)

FIG. 3. Gray scale STM images of type-II structures, windows of 780×780 Å^2; z range: 44 Å.

placement energy of 31 eV for graphite[14] and a surface binding energy of 7.3 eV, after 2.2×10^6 incident ions, yielded a value of 6.1×10^{-5} backsputtered C atoms/incident ion.

Three types of surface features were found. Type-I features consist of hillocks with irregular shapes and irregular height distributions. A typical example is shown in Fig. 1. Several satellites may be observed around a central main hillock. As it is very likely that they originated from the same knocked-on C atom which had produced a nuclear cascade in the surface region, they are considered as a single event. Typical dimensions of type-I features are diameter 100–300 nm and height 3–7 nm. It was possible to achieve atomic resolution on the top part of some of type-I features. A short-range graphitelike order was observed, but the distortions of the lattice destroyed long-range order. As can be seen in Fig. 2, the lattice superimposed on the atomic resolution image is in satisfactory coincidence only in the upper right-hand part of the image. The lattice parameters are $A1=0.247$ nm, $A2=0.24$ nm, and $\theta=65.4°$. A similar lattice with a slightly different orientation may be superimposed on the lower left-hand part of the image.

Type-II structures consist of elliptically shaped features with a constant height of about 2.5 nm over the nonaltered HOPG surface. A well-developed crater with ≈1.5-nm depth measured from the original HOPG surface is observed in type-II structures. The crater is placed asymmetrically along the major axis of the ellipse, i.e., closer to one of the ends. Figures 3(a) and 3(b) show two features of this type. One can observe that the craters themselves are elongated in the same direction as the type-II structures. The diameter of the craters at the level of the nonaltered HOPG surface is in the range of 10–15 nm, while the size of the type-II features is of 50 nm in the smaller diameter and around 100 nm in the larger one.

Figure 4(a) shows a line cut along the major axis of a type-II structure, and Fig. 4(b) shows a horizontal line cut through the crater of the same structure. The height of the type-II structure is relatively constant over several hundred Å. In Fig. 5(a), an image is shown taken with atomic resolution in the vicinity of the crater. A slightly disturbed graphitelike lattice is present in the lower half of the image. The line cut in Fig. 5(b) shows that although the periodicity is preserved, the corrugation is not as regular as one would expect over the unperturbed HOPG. The lattice parameters in this region are $A1=0.246$ nm, $A2=0.239$ nm, and $\theta=59.9°$, respectively.

The type-III structure is a regular superstructure with graphitelike symmetry. The lattice parameters of the superstructure are $A1=20.3$ nm and $A2=17.3$ nm, re-

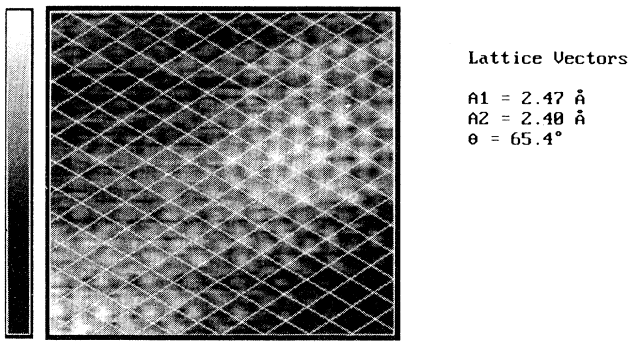

FIG. 2. Atomic resolution STM image on the top of a type-I structure; window of 32×32 Å^2. A graphitelike lattice with $A1=2.47$ Å, $A2=2.40$ Å, and $\theta=65.4°$ is superimposed over the recorded image.

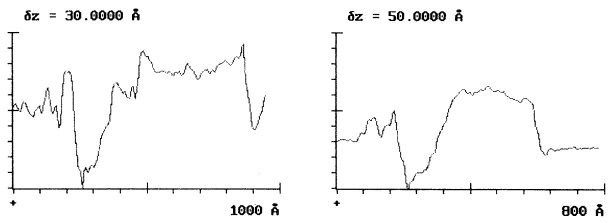

a) b)

FIG. 4. Line cuts over the type-II structure in Fig. 3(a): (a) Line cut along the major axis. (b) Horizontal line cut through the crater.

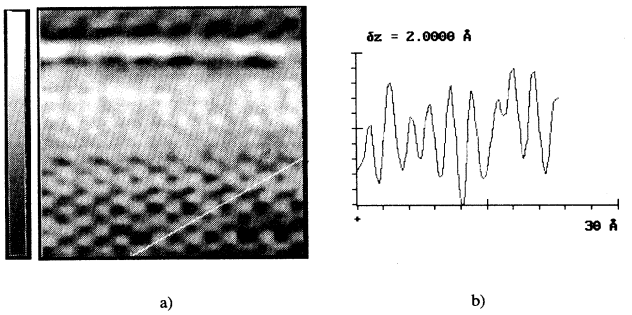

a) b)

FIG. 5. Atomic resolution STM image near the crater of the type-II structure shown in Fig. 3(a): (a) Plan view; window of 30×30 Å^2; z range: 5.8 Å. (b) Line cut showing the corrugation along the white line indicated in (a); the cross marks the starting point.

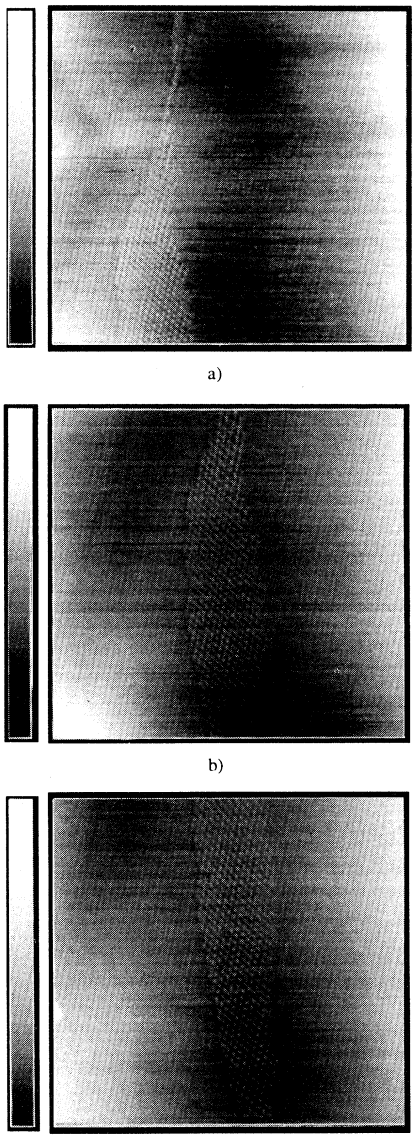

a)

b)

c)

FIG. 6. Gray scale STM images of a type-III structure; windows of 7000×7000 Å^2; z range: 7.5 Å. (a) Starting part. (b) Middle part. (c) Ending part.

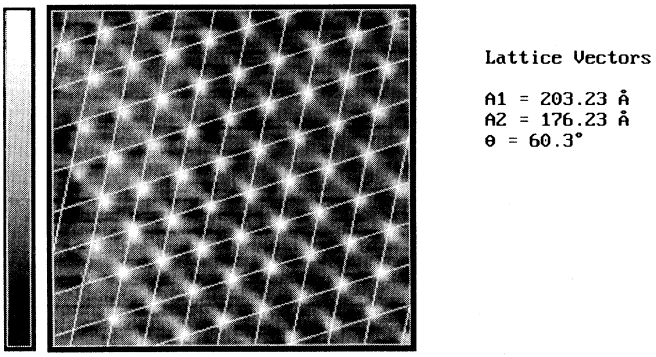

FIG. 7. Lattice superimposed over a detail of the type-III structure shown in Fig. 6; window of 1500×1500 Å^2; z range: 4.1 Å. Lattice vectors $A1=203.23$ Å, $A2=176.23$ Å, and $\theta=60.3°$.

spectively, with an angle of 60.3°. The 14% difference between the two lattice vectors may be attributed to drift during scanning due to the reduced scanning velocity used. The maximum width of the superstructure is of the order of 150 nm, while its estimated length is 1500 nm. The height of one element of the superstructure is in the range of 0.15–0.3 nm. In Figs. 6(a), 6(b), and 6(c) the beginning, middle, and end parts of the superstructure are shown, respectively. A lattice with parameters, mentioned earlier, is superimposed over a detail of the superstructure as shown in Fig. 7. In Fig. 8(a), a detail of the

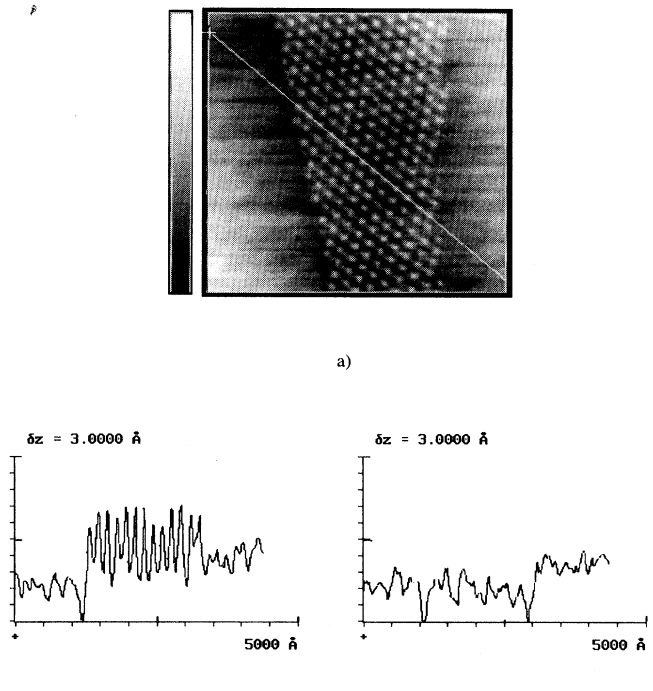

a)

b) c)

FIG. 8. Detail of the type-III structure shown in Fig. 6; window of 3280×3280 Å^2; z range: 3.8 Å. (a) Gray scale plan view. (b) Line cut along the white line in (a); the cross indicates the starting point. (c) Line cut between two rows of maxima.

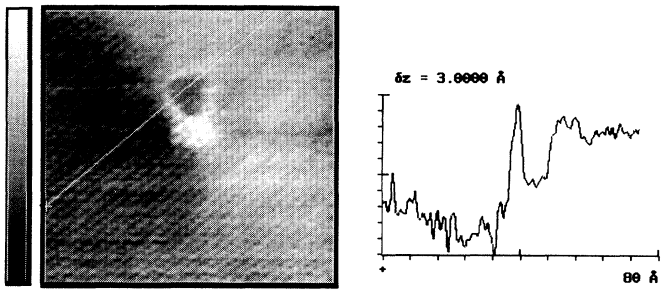

a) b)

FIG. 9. Atomic resolution detail of the superstructures shown in Fig. 6; the lighter right-hand upper corner corresponds to a superstructure maximum; window of 68×71 Å^2; z range: 4.6 Å. (a) Plan view image. (b) Line cut over the white line indicated in (a); the cross marks the starting point.

superstructure is shown. The white line indicates the position of the line cut shown in Fig. 8(b). In Fig. 8(c), a parallel line cut is shown which was taken between two rows of maxima, one of the rows the one through which the line cut in Fig. 8(b) was taken. As the distance between two c planes of the graphite structure is 0.335 nm, it is very unlikely that the superstructure is a result of even one atomic layer thick graphite flake lying over the HOPG sample. At the end part of the superstructure in some points, small craterlike features were observed. In Fig. 9(a), a crater of this type is shown. As one can see from the line cut in Fig. 9(b), the depth of the crater is about 0.15 nm. This suggests that atoms are missing only from the uppermost atomic layer of the sample. These craters were usually found on the edge of the superstructure in association with the maxima of the superstructure. It should be mentioned that these craters may be formed where low-energy C atoms are ejected from the surface.

DISCUSSIONS

A surprising observation is the lack of entrance features due to the bombarding ion impacts. The probable reason for this is the relatively low values of the electronic and nuclear stopping powers of the Ne ions. For the 215-MeV Ne ions the value of the electronic stopping is 8.6×10^2 keV/μm, a factor of 2 lower than the maximum in the 10-MeV range. The nuclear stopping power is close to zero at 215 MeV, so the energy deposited at the surface may be insufficient for entrance feature formation. The event that a high-energy Ne in deeper regions of the target changes the direction of motion by more than 90° has an extremely reduced probability, so the surface features observed have to be attributed to knocked-on C atoms of different energy ranges.

In conditions of the present experiment in the region close to the surface, C atoms may gain high enough kinetic energy to leave the lattice position by several mechanisms: (i) nuclear collisions, (ii) by Coulomb explosion,[8] and (iii) by the thermal-ionization spike mechanisms.[15]

The kinetic energy transmitted to the knocked-on atom in a hard-sphere elastic-scattering model is given by

$$E_r = E_0[4M_1M_2/(M_1+M_2)^2]\cos^2\theta \ , \tag{1}$$

where θ is the angle between the direction of the incident particle and the direction in which the knocked-on particle moves; M_1 and M_2 are the atomic masses of the projectile and target atoms, respectively; and E_0 is the incident energy. Any C atom reaching the target surface is generated in a secondary or higher-order collision. For the case of a secondary collision, the sum $\theta_1+\theta_2>\pi/2$, for an atom leaving the sample surface, or $\theta_1+\theta_2=\pi/2$, for an atom moving parallel with the ample surface, and θ_1 and θ_2 stand for the first and second collisions, respectively. This is a necessary, but not a sufficient condition because the secondary knocked-on atom is free to move with equal probability under any azimuthal angle around the direction defined by the trajectory of the primary knocked-on atom (PKA). The highest possible amount of energy transferred to the secondary knocked-on C atom will be 50.3 MeV for a recoil particle moving parallel to the sample surface. This value is on the high-energy side of the electronic stopping maximum of C in C situated at 2.6 MeV.

A second alternative is the occurrence of a Coulomb explosion.[8] The effects that may arise because of electric charges accumulated on the nuclei along the ion track depend on several factors, but the two most important ones are the degree of ionization, i.e., the number of electrons lost by one atom; and how long this charged state will sustain before it is neutralized.

Carbon loses the first four electrons relatively easily, the ionization energy required to create a C^{4+} ion being 64.5 eV. It is more difficult to estimate the lifetime of the charged state. It is well known that the electrical conductivity of graphite is about three orders of magnitude higher in the c plane than in a direction perpendicular to it.[16] The strong anisotropy originates from the structure of graphite; within the c plane each carbon atom is in an sp^2 hybridized state, and bonded to other three carbon atoms. The nonbonded p_z atomic orbitals overlap to give a completely delocalized system of molecular orbitals, thus allowing the transport of electrons through the crystal. The density of charge carriers in graphite is in the range of 10^{18} cm^{-3} (Ref. 16). This value is two orders of magnitude below the threshold for charge-carrier density over which Coulomb explosion effects cannot be expected.[8] So, due to the relatively low energy needed for multiple ionization, to the strong anisotropy of electrical properties, and to charge-carrier densities below the threshold, Coulomb explosion effects are not excluded in HOPG. However, the potential energy stored between two C^{4+} atoms at a distance of 0.142 nm is only of the order of 2.6 keV. This energy is too small for the production of swift particles (stopping in the electronic range), even in the case when several neighboring atoms are ionized and collective effects are considered, but it may be enough for the production of the crates observed in type-

II structures.

The thermal-ionization spike model provides an alternative mechanism for damage formation by electronic excitation.[15] According to this, a hot region—where the temperature may well exceed the melting temperature of the material—is produced along the ion trajectory on a time scale of picosecond order. The effects of this high-temperature–high-pressure cylinder are close to those expected for Coulomb explosion effects. As, by STM examination of the surface, one can hardly make a clear distinction between the Coulomb explosion or thermal-ionization spike effects, no separate treatment will be done.

The production of type-I structures may be attributed to knocked-on C atoms with energies in the range of 10 keV. Below this value the nuclear stopping becomes dominant over the electronic stopping, so any further knocked-on C atom will lose its energy dominantly by nuclear displacements. The conditions that must be fulfilled for the production of a type-I structure are as follows: (i) the creation in the surface region of a PKA with energy in the range of 10 keV s or higher; (ii) one of the secondaries generated, with high enough energy, has to move towards the surface; and (iii) in the region close to the surface there numerous higher-order knocked-on particles must be produced with energies in the keV range; overlapping cascades of individual particles will generate the type-I structure.

Care should be exerted if one tries to estimate the energy deposited during the formation of a type-I structure. Energy sufficient to produce the structure will be only a fraction of the total energy of the whole cascade. If one considers a feature which can be enclosed a cylinder with a radius of 150 nm and a height of 10 nm, the value of the heat of sublimation (the surface binding energy for graphite), 7.3 eV, will render the energy of 600 eV necessary to create the structure. This is very likely an overestimation, because this amount of energy would produce its sublimation provided the heat conduction was neglected. On the other hand, a dominant amount of energy has been deposited in the deeper regions of the cascade, so the total energy released during the nuclear cascade production, including the deep parts of the cascade, will be well over 600 eV. Energy values up to two orders of magnitude higher, i.e., 60 keV for knocked-on C atoms, do not seem to be unrealistic under the conditions of the present experiment. Analytical calculations using the LET code,[17] for 215-MeV Ne implanted in C, show that about 10% of the PKA's (primary knocked-on atoms) have an energy in the 60-keV to MeV range. Certainly, only a fraction of these high-energy PKA's will generate secondaries able to reach the surface.

If one assumes a C foil of ten atomic layers, the TRIM simulation gives a 50% transmission probability for 1-keV C particles, i.e, half of the particles will deposit their total energy within this layer. In conclusion, type-I structures are attributed to C atoms with energies in the nuclear stopping range, and the structure is a result of several overlapping cascades which are of common origin and have energies in the keV range. If the knocked-on atom has an energy over 20 keV, cascades tend to split to the subcascades.[18] The satellites observed are a result of deeper cascade branching, where C atoms were displaced in a way that their orientation is different from the direction of the main cascade, but also pointing toward the surface.

The number vs energy of sputtered C atoms given by the TRIM simulation shows that 75% of the C atoms leave the surface with energies less than 500 eV. This means that they must have created (and originated from) nuclear cascades, i.e., type-I structures. This is in agreement with the experiment, as the most frequently found structures are of type I.

The short-range graphitelike orders found over type-I features may be attributed to the conservation to a certain extent of the graphite structure in the damaged region. It is well known that the disordering of graphite is associated with the increase in the spacing of c layers,[16] and the most disorganized structures of graphite are composed of 2.5-nm graphite grains randomly oriented with respect to each other, and are turbostratic[19] in the layer arrangement. A paper on 200-keV e-beam-irradiated graphite[20] showed that one of the consequences of irradiation is bending and randomization of the c planes of graphite. Even cross-linking, i.e, the connecting of different c planes, is possible. In those type-I structures on which atomic resolution may be achieved, the layered order is preserved to a certain extent; this explains the possibility of atomic resolution images with HOPG structures, but the long-range order is destroyed. The existence of a graphitelike structure excludes features such as impurity particles sticking to the sample surface.

Type-II structures are attributed to swift particles with stopping in the electronic range, and which have a trajectory that intersects the surface. If the direction in which the particle moves is perpendicular to the surface, one would expect a circular feature. The production mechanism of type-II structures is shown schematically in Fig. 10. The displacement of surface layers is a consequence of the pressure-temperature pulse that reaches the surface within the electronic cascade. The crater corresponds to the dense core of the electronic cascade from which C atoms are ejected due to Coulomb explosion or thermal-ionization spike effects.

Similar surface structures were observed by atomic-force-microscopy (AFM) examination on 78.2-MeV iodine-irradiated L-valine crystals.[21] These surface structures were produced by ions entering the target, with a stopping power of 1.5×10^4 keV/μm; this value is about 20 times higher than 8.68×10^2 keV/μm, the stopping power of 215-MeV Ne in C. The stopping power of C in

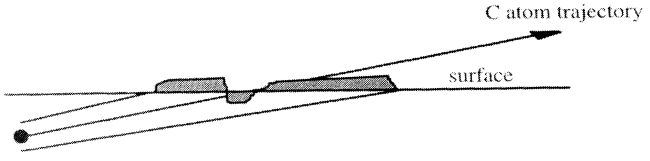

FIG. 10. Schematic mechanism for the production of a type-II structure. The shaded areas indicate the regions where the surface modifications are produced.

C peaks at 2.6 MeV is 1.7×10^3 keV/μm. This value is about twice as high as the value of Ne ions entering the target. As shown by earlier transmission-electron-microscopy pictures of $YBa_2Cu_3O_{7-\delta}$ irradiated with high-energy ions, variations of the electronic stopping by a factor of 2 can produce a significant alteration of damage morphology.[22] The increase of electronic stopping power from 1.1×10^3 to 2.8×10^3 keV/μm caused the change from insulated spherical damage regions to elongated columnar damage regions. AFM investigation of traces produced in mica by swift Kr ions also indicate the existence of a clear threshold at 3.4×10^3 keV/μm for damage observation.[23] However, a systematic investigation of surface damage vs impinging ion energy is necessary to find the threshold value of damage production by electronic stopping in HOPG.

The surface structure reported on *L*-valine irradiated under a gazing incidence of 79° (Ref. 21) show craters with tails; i.e., the crater is followed by elevated regions of the surface along the ion trajectory. The production of the crater and tail is attributed to a cylindrical pressure pulse along the ion trajectory.

The mechanism of crater production has been investigated by several workers and several methods. Irrespective of the method used—analytical calculation[24,25] or computer simulation[26,27]—it turns out that during the passage of an energetic ion in the cylindrical track characterized by high excitation of the particles, a certain amount of the energy may be converted into center-of-mass motion in a short time (of the order of $10^{-13}-10^{-12}$ s). This can give rise to a transiently pressurized cylindrical disturbance, which at the vacuum interface will cause the ejection of material. Where the pressure is below a certain threshold the effect will be only the modification of surface topography without material ejection.

In the case of the present experiment, type-II structures are attributed to knocked-on C atoms leaving the target, and not to the bombarding Ne ions. There are several reasons that support this assumption. First, the low values of stopping for 215-MeV Ne would not permit sufficient energy deposition in the first few atomic layers at the surface. Second, the irradiation was carried out at normal incidence, so the features produced by ions entering the target, if any, should have circular symmetry, as found in Ref. 21. Third, only a few type-II structures were found; if the entering ions are the cause of this type of structure, they should have a density in the range of the dose. Last, but not least, the geometry of the structure [(i) the position of the crater with respect to the center of the ellipse, Fig. 3(a); (ii) the direction in which the crater is broadened (broadening is expected in the direction in which the ejected material propagates); and (iii) the coincidence of the broadening direction of the crater with the less steep side of the crate, Fig. 4(a)] is in agreement with the production mechanism shown schematically in Fig. 10.

The dimensions of type-II structures are in correlation with data reported earlier,[20] and with the commonly accepted values of the dimensions of the region influenced by Coulomb explosion effects.

Very clear differences between type-I and II structures show that the two different damage production mechanisms (nuclear or electronic stopping) produce very different damage structures on the surface of HOPG.

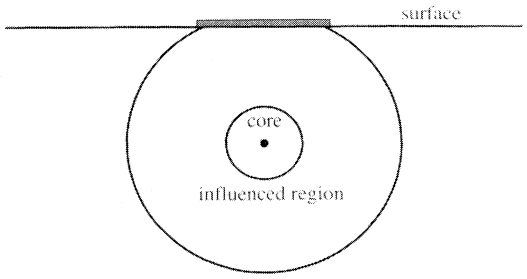

FIG. 11. Schematic mechanism for the production of a type-III structure. The C atom enters the plane of the paper. The shaded region marks where the superstructure is expected.

A possible mechanism for the creation of a type-III structure is that, in contrast to type II, the knocked-on C atom moves parallel to the sample surface at a depth of a few atomic layers. As shown in Fig. 11, the surface is far from the core of the track, as it is on the edge of the influenced region. The energy deposited at the surface is not enough to produce massive atomic displacements in a direction perpendicular to the surface, but due to the pressure and heat effects it may produce structural modification of the graphite layers that were subjected to the effects of the passing ion.

Large-scale periodic features on HOPG were reported earlier under different experimental conditions.[6,28–30] They were interpreted as Moiré-like effects due to rotational misorientation of graphite layers.[29,30] An alternative explanation is suggested in Ref. 29, based on shortening of bond lengths in the top layer of graphite by a few percent. Both effects seem possible in the region exposed to temperature and pressure effects of the swift ion. The comparison of STM and AFM examinations of superstructures resulted after bombardment of HOPG with 2.82-MeV/*a* U ions suggests that the superstructures observed are not topographic, but electronic effects.[6]

The following mechanism is proposed for the production of type-III structure: (i) a knocked-on C atom, with the energy in the MeV range moving parallel to the surface, is generated in the vicinity of the surface; (ii) as the C atom slows down to energies in the range of maximum of electronic stopping, the diameter of the influenced region grows, and at a certain point it reaches the surface; and (iii) below 2.6 MeV, the diameter of the influenced region decreases. This scenario is in good agreement with the variation in the dimensions of the type-III structure shown in Figs. 6(a), 6(b), and 6(c). The fast increase in the width of the structure in the starting region is followed by a slower decrease of the width in the ending part. This is how dimensions of the influenced region are expected to change in the region of the electronic stopping maximum. The exit points observed in the end part o the type-III structure may be caused either by local fluctuations in the energy distribution at the surface, so that the ejection or evaporation of a small cluster is possi-

ble, or to some low-energy C atoms produced by nuclear collisions. The occurrence of exit points at the beginning of the cascade was not checked systematically.

CONCLUSIONS

Due to the broad energy spectrum of PKA's in the case of very high-energy irradiation, which produces knocked-on C atoms up to MeV energies, it was possible to observe on the same sample surface features produced by low-energy knocked-on atoms and features attributable to atoms with MeV energy. STM examination of HOPG irradiated by 215-MeV Ne revealed three types of structures: type I, produced by cascades of knocked-on C atoms with dominant nuclear stopping; type II, produced by cascades of knocked-on C atoms with dominant electronic stopping crossing the surface; and type III, attributed to a knocked-on C atom with an energy around the maximum of electronic stopping which moved parallel with the surface. Features attributable to entering Ne ions were not observed.

The differences found in type-I and -II features show that defects produced on the surface of HOPG by nuclear and electronic cascades can be clearly distinguished.

The proposed production mechanism of type-I structures raises the question of whether the so-called hillocks, commonly observed during low- and medium-energy irradiation of HOPG and usually attributed to the bombarding ions themselves, are produced by the ions entering the target, or by knocked-on target atoms leaving the target.

A good agreement was found between the experimental density of surface features and the number of backsputtered C atoms given by the TRIM code.

ACKNOWLEDGMENTS

The work was supported by OTKA Grant No. 3265 in Hungary. Sample irradiations were possible due to an agreement between the Hungarian Academy of Sciences and the Joint Institute for Nuclear Research, Dubna, Russia.

[1]J. H. W. Simmons, *Radiation Damage in Graphite* (Pergamon, Oxford, 1965).
[2]R. Coratger, A. Claverie, F. Ajustron, and J. Beauwillain, Surf. Sci. **227**, 7 (1990).
[3]L. Porte, M. Phaner, C. H. de Villeneuve, N. Moncoffre, and J. Tousset, Nucl. Instrum. Methods Phys. Res. Sect. B **44**, 116 (1989).
[4]L. Porte, C. H. de Villeneuve, and M. Phaner, J. Vac. Sci. Technol. B **9**, 1064 (1991).
[5]H. Kang, K. H. Park, C. Kim, B. S. Shim, S. Kim, and D. W. Moon, Nucl. Instrum. Methods Phys. Res. Sect. B **67**, 312 (1992).
[6]S. Boufard, J. Coutsy, Y. Pennec, and F. Thibaudau, Radiat. Eff. Defects **126**, 225 (1993).
[7]Y. Junjue, Z. Li, C. Bai, W. S. Yang, Y. Wang, W. Zhao, Y. Kang, F. C. Yu, P. Zhai, and X. Tang, J. Appl. Phys. **75**, 1390 (1994).
[8]R. L. Fleischer, P. B. Price, and R. M. Walker, J. Appl. Phys. **36**, 3645 (1965).
[9]B. E. Fischer and R. Spohr, Rev. Mod. Phys. **55**, 907 (1983).
[10]A. Dunlop, P. Legrand, D. Lesueur, N. Lorenzelli, J. Morrillo, A. Barbu, and S. Bouffard, Europhys. Lett. **15**, 765 (1991).
[11]H. Dammak, A. Barbu, A. Dunlop, D. Leusuer, and N. Lorenzelli, Philos. Mag. **67**, 253 (1993).
[12]A. Dunlop, D. Lesueur, and A. Barbu, J. Nucl. Mater. **205**, 426 (1993).
[13]J. F. Ziegler, J. P. Bierack, and U. Littmart, *The Stopping and Ranges of Ions in Solids* (Pergamon, New York, 1985), Vol. 1.
[14]F. W. Clinard and L. W. Hobbs in *Physics of Radiation Effects in Crystals,* edited by R. A. Johnson and A. N. Orlov (North-Holland, Amsterdam, 1986), p. 392.
[15]D. A. Thompson, Radiat. Eff. **56**, 105 (1981).
[16]C. A. Klein, Rev. Mod. Phys. **34**, 56 (1962).
[17]G. Bárdos, Phys. Lett. A **119**, 415 (1987).
[18]W. Wiedersich, Nucl. Instrum. Methods Phys. Res. Sect. B **205**, 40 (1993).
[19]P. L. Walker, *Chemistry and Physics of Carbon* (Marcel Dekker, New York, 1971), Vol. 7, p. 9.
[20]T. Tanabe, S. Muto, and K. Niwase, Appl. Phys. Lett. **61**, 1638 (1992).
[21]J. Kopniczky, C. T. Reinmann, A. Hallén, B. U. R. Sundqvist, P. Tengvall, and R. Erlandsson, Phys. Rev. B **49**, 625 (1994).
[22]R. Wheeler, M. A. Kirk, A. D. Marwick, L. Clivale, and H. Holtzberger, Appl. Phys. Lett. **63**, 1573 (1993).
[23]F. Thibaudau, J. Cousty, E. Balanzat, and S. Bouffard, Phys. Rev. Lett. **67**, 1582 (1991).
[24]I. S. Bitensky and E. S. Parilis, Nucl. Instrum. Methods Phys. Res. Sect. B **21**, 26 (1987).
[25]R. E. Johnson, B. U. R. Sundqvist, A. Hedin, and D. Fenyö, Phys. Rev. B **40**, 49 (1989).
[26]D. Fenyö, B. U. R. Sundqvsit, and B. R. Karlsson, Phys. Rev. B **42**, 41 (1990).
[27]D. Fenyö and R. E. Johnson, Phys. Rev. B **46**, 5090 (1992).
[28]M. Kuwabara, D. R. Klarke, and D. A. Smith, Appl. Phys. Lett. **56**, 2396 (1990).
[29]J. E. Buckley, J. L. Wragg, H. W. White, A. Bruckforder, and D. L. Worchester, J. Vac. Sci. Technol. B **9**, 1079 (1991).
[30]J. Xhie, K. Sattler, M. Ge, and N. Vekkateswaran, Phys. Rev. B **47**, 15 835 (1993).

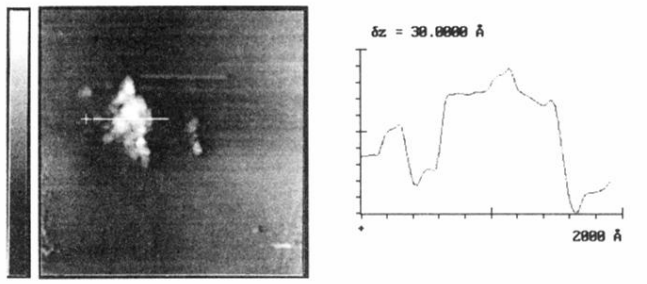

FIG. 1. Gray scale STM image; window of 6100×6100 Å^2; z range: 35 Å. The gray scale on the left side corresponds to the whole z range. (a) Plan view of a type-I structure. (b) Line cut along the white line in (a); the cross indicates the starting point.

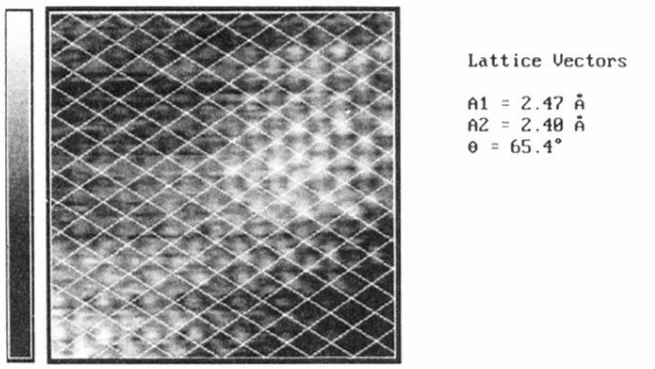

FIG. 2. Atomic resolution STM image on the top of a type-I structure; window of 32×32 Å^2. A graphitelike lattice with $A1=2.47$ Å, $A2=2.40$ Å, and $\theta=65.4°$ is superimposed over the recorded image.

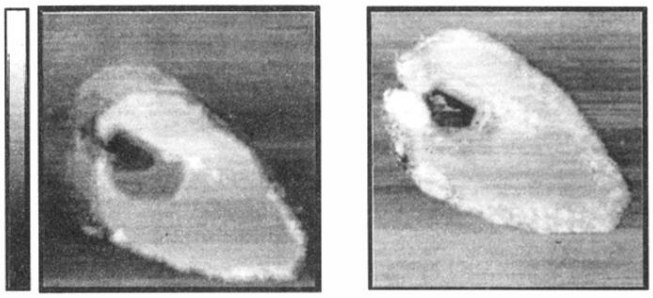

a) b)

FIG. 3. Gray scale STM images of type-II structures, windows of 780×780 Å^2; z range: 44 Å.

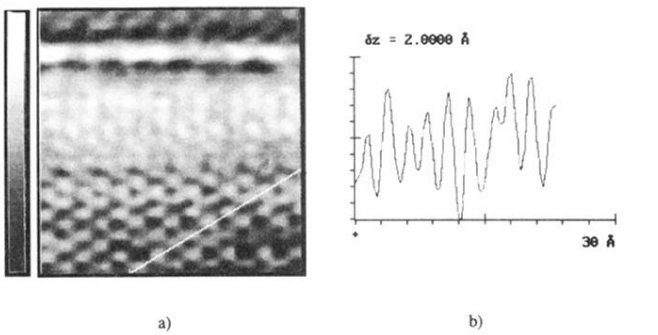

a) b)

FIG. 5. Atomic resolution STM image near the crater of the type-II structure shown in Fig. 3(a): (a) Plan view; window of 30×30 Å^2; z range: 5.8 Å. (b) Line cut showing the corrugation along the white line indicated in (a); the cross marks the starting point.

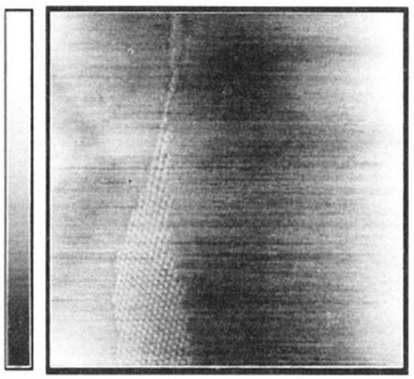

a)

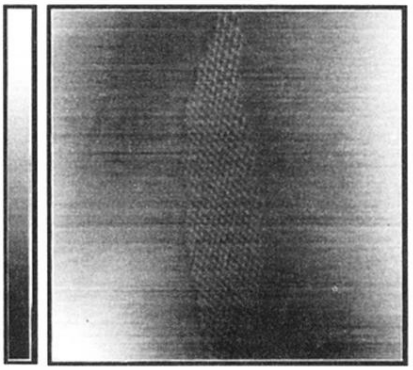

b)

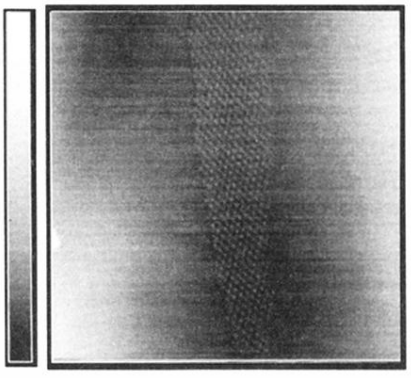

c)

FIG. 6. Gray scale STM images of a type-III structure; windows of 7000×7000 Å^2; z range: 7.5 Å. (a) Starting part. (b) Middle part. (c) Ending part.

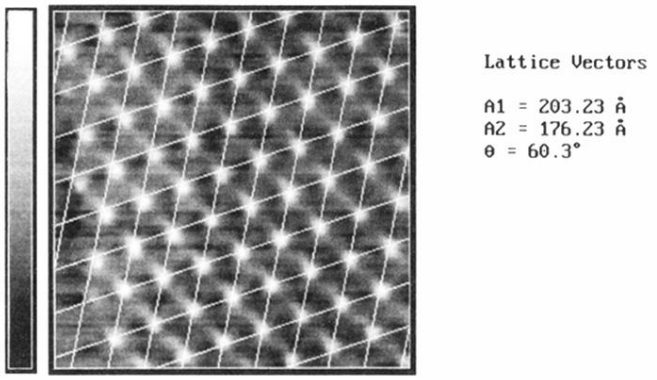

FIG. 7. Lattice superimposed over a detail of the type-III structure shown in Fig. 6; window of 1500×1500 Å^2; z range: 4.1 Å. Lattice vectors $A1 = 203.23$ Å, $A2 = 176.23$ Å, and $\theta = 60.3°$.

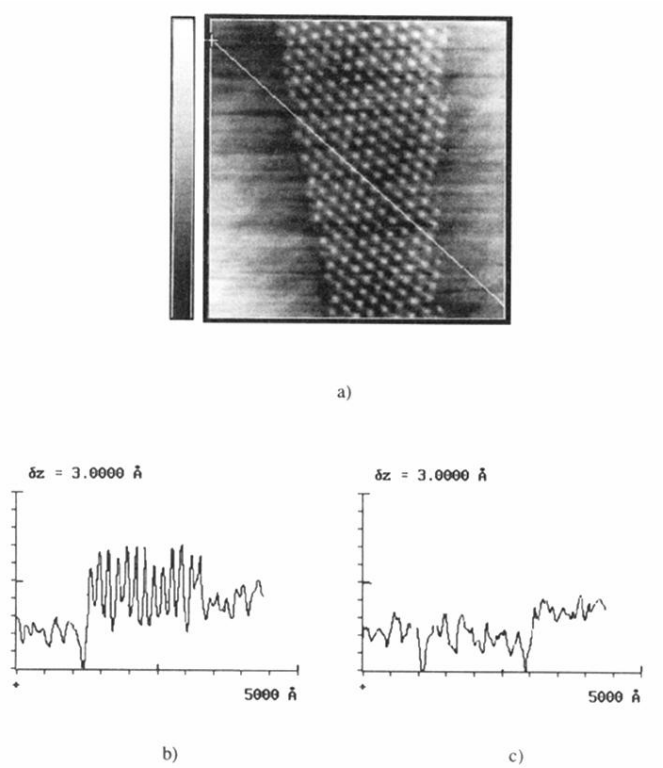

FIG. 8. Detail of the type-III structure shown in Fig. 6; window of 3280×3280 Å^2; z range: 3.8 Å. (a) Gray scale plan view. (b) Line cut along the white line in (a); the cross indicates the starting point. (c) Line cut between two rows of maxima.

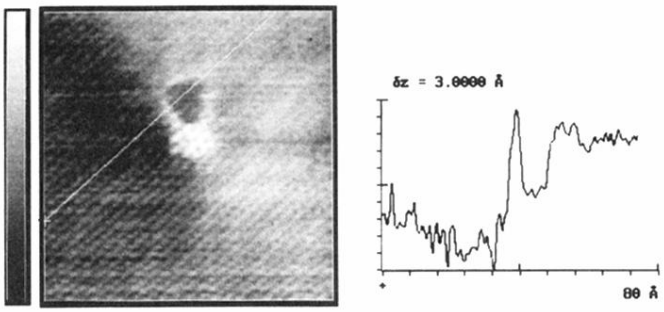

a) b)

FIG. 9. Atomic resolution detail of the superstructures shown in Fig. 6; the lighter right-hand upper corner corresponds to a superstructure maximum; window of 68×71 Å^2; z range: 4.6 Å. (a) Plan view image. (b) Line cut over the white line indicated in (a); the cross marks the starting point.